Geophysical Research Letters

RESEARCH LETTER
10.1029/2020GL090736

Fault-Zone Damage Promotes Pulse-Like Rupture and Back-Propagating Fronts via Quasi-Static Effects

B. Idini[1] **and J.-P. Ampuero**[2]

[1]Seismological Laboratory, California Institute of Technology, Pasadena, CA, USA, [2]Université Côte d'Azur, IRD, CNRS, Observatoire de la Côte d'Azur, Géoazur, Valbonne, France

Key Points:
- Highly damaged fault zones promote pulse-like ruptures even without the dynamic effects of reflected waves
- Slip complexity induced by fault damage involves multiple back-propagating rupture fronts
- A new mechanism for rapid tremor reversals is observed during episodic tremor and slip

Supporting Information:
- Supporting Information S1

Correspondence to:
B. Idini,
bidiniza@caltech.edu

Citation:
Idini, B., & Ampuero, J.-P. (2020). Fault-zone damage promotes pulse-like rupture and back-propagating fronts via quasi-static effects. *Geophysical Research Letters*, *47*, e2020GL090736. https://doi.org/10.1029/2020GL090736

Received 9 SEP 2020
Accepted 5 NOV 2020
Accepted article online 9 NOV 2020

Abstract Damage zones are ubiquitous components of faults that may affect earthquake rupture. Simulations show that pulse-like rupture can be induced by the dynamic effect of waves reflected by sharp fault zone boundaries. Here we show that pulses can appear in a highly damaged fault zone even in the absence of reflected waves. We use quasi-static scaling arguments and quasi-dynamic earthquake cycle simulations to show that a crack turns into a pulse after the rupture has grown larger than the fault zone thickness. Accompanying the pulses, we find complex rupture patterns involving back-propagating fronts that emerge from the primary rupture front. Our model provides a mechanism for back-propagating fronts recently observed during large earthquakes. Moreover, we find that slow-slip simulations in a highly compliant fault zone also produce back-propagating fronts, suggesting a new mechanism for the rapid tremor reversals observed in Cascadia and Japan.

Plain Language Summary Damage zones are zones of fractured rock that surround faults and can influence how earthquakes propagate. Previous computer models show that damage zones promote an inchworm-like (rather than zipper-like) pattern of earthquake propagation, known as pulses. This finding has been previously attributed to the effect of seismic waves reflected at the boundaries of the damage zone. Here, we show that pulses are generated in highly fractured damage zones independently of the reflection of seismic waves. We reach this conclusion by scaling arguments confirmed by numerical simulations of sequences of earthquakes in which we ignore the reflection of seismic waves. Moreover, our models produce an unexpected pattern of earthquake propagation: Secondary rupture fronts emerge from the primary rupture front and propagate in the opposite direction. Similar back-propagating fronts have been previously observed during slow earthquakes in subduction zones and more recently during large earthquakes. Our work reveals a possible connection between an observable structural feature of faults and complicated patterns of earthquake propagation.

1. Introduction

Pulse-like rupture (hereafter referred to as pulses) is a common mode of earthquake propagation in which the duration of slip at each point of the fault, known as the rise time, is short compared to the total rupture duration (Heaton, 1990). Pulses play a prominent role in the theory of earthquake mechanics: They can radically affect the earthquake energy balance (Nielsen & Madariaga, 2003), reduce the apparent strength of faults (Noda et al., 2009), enhance the spatial heterogeneity of earthquake slip and stress (Aagaard & Heaton, 2008), and promote complexity of seismicity manifested by a broad range of event magnitudes (Cochard & Madariaga, 1996). Yet, their origin is not completely established. Several mechanisms of pulse generation have been proposed, involving healing fronts emerging from features of the friction law (Cochard & Madariaga, 1996; Perrin et al., 1995), from early arrest of one dimension of rupture (Day, 1982; Johnson, 1990), from fault heterogeneities (Beroza & Mikumo, 1996; Day et al., 1998), or from waves reflected in a low-velocity fault damage zone (Huang & Ampuero, 2011). The present work focuses on the generation of pulses by damaged zones.

Faults are usually embedded in a damaged zone (Figure 1a) characterized in field observations by distributed fractures and micro-cracks (Chester & Logan, 1986; Mitchell & Faulkner, 2009; Savage & Brodsky, 2011) and in seismological and geodetic observations by reduced wave speeds or elastic modulus relative to the host rock (Ben-Zion et al., 2003; Cochran et al., 2009; Lewis & Ben-Zion, 2010; Lewis et al., 2005; Li et al., 1990, 2002, 2006, 2007; Mizuno et al., 2008; Peng et al., 2003; Yang & Zhu, 2010; Yang et al., 2011).

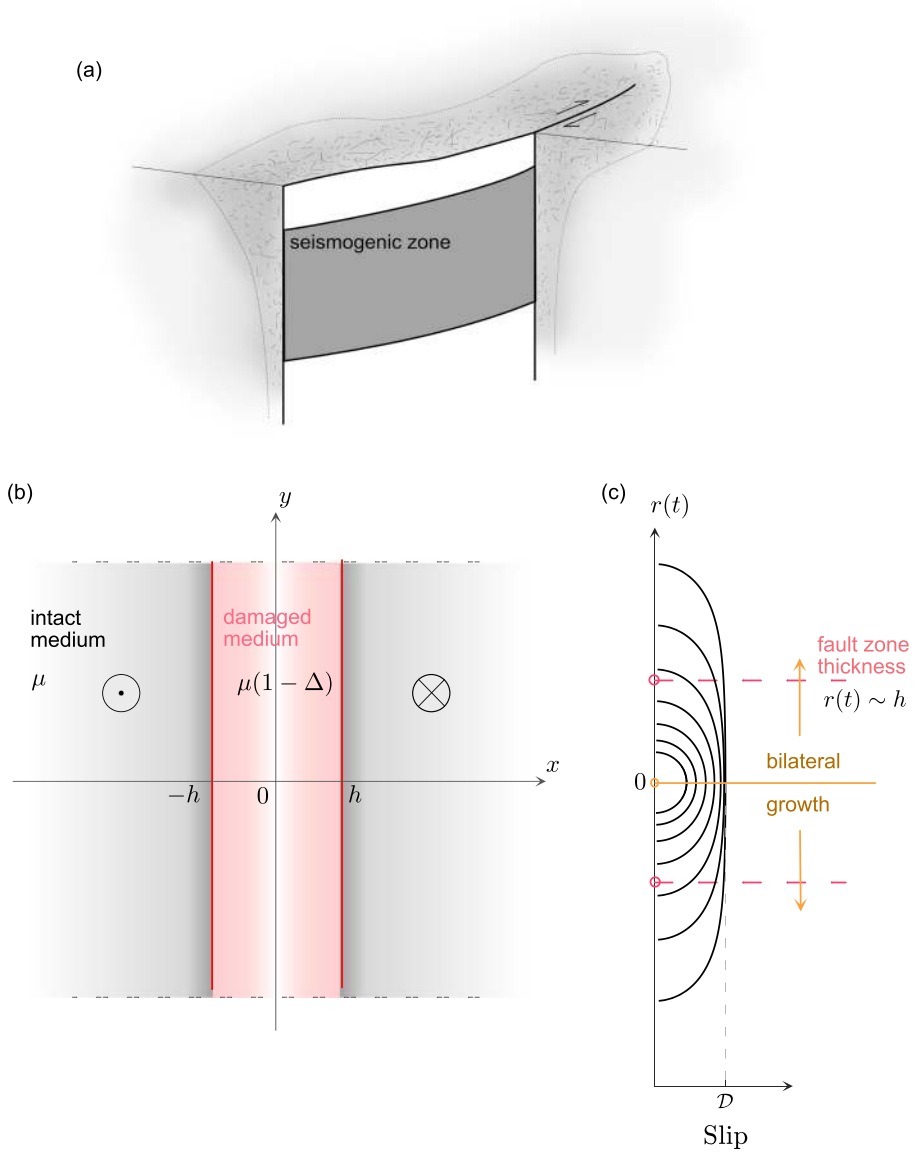

Figure 1. (a) Schematic representation of a fault zone. (b) Conceptualization of a fault zone as a simple tabular low-velocity fault zone (LVFZ) model. The damaged and intact media have constant shear modulus, $(1-\Delta)\mu$ and μ, respectively. (c) Quasi-static rupture growth with uniform stress drop in a LVFZ, showing a transition from crack-like (elliptical) to pulse-like (flat) slip profiles when the rupture length exceeds the LVFZ thickness. The static slip profiles are computed numerically for $\Delta = 0.99$ by the method described in Text S2.

Seismic imaging methods resolve fault zones of strike-slip faults as flower structures with depth-varying thickness and damage (Ben-Zion et al., 2003; Finzi et al., 2009). Hereafter, we refer to these structures as low-velocity fault zones (LVFZs).

Dynamic rupture simulations show that the presence of a LVFZ can induce complex rupture patterns: pulses promoted by healing fronts mediated by reflected waves, oscillations of slip rate and rupture speed, and supershear rupture at low background stress (Harris & Day, 1997; Huang & Ampuero, 2011; Huang et al., 2014, 2016). Recent earthquake cycle simulations show that the generation of pulses by an LVFZ is persistent across multiple earthquake cycles, both in fully dynamic (Thakur et al., 2020) and quasi-dynamic simulations (Idini & Ampuero, 2017). The mechanism of pulse generation by a LVFZ has been previously attributed to the dynamic effect of waves reflected at the boundary of the LVFZ, which tend to unload the fault and promote slip arrest (Huang & Ampuero, 2011; Thakur et al., 2020). However, LVFZ quasi-dynamic

simulations do not include these reflected waves. Here, we explain how pulses can be promoted in LVFZs by a quasi-static mechanism.

The present work is further motivated by recent evidence of complex rupture patterns in earthquakes and tectonic tremors, in particular back-propagating fronts. While the inherent complexity of large earthquakes is abundantly highlighted by modern seismological observations (Meng et al., 2012; Ross et al., 2019), reports of secondary rupture fronts propagating in the direction opposite to the main front (i.e., towards the hypocenter) are becoming increasingly clear and robust (Beroza & Spudich, 1988; Hicks et al., 2020; Meng et al., 2011; Uchide et al., 2013; Vallée et al., 2020). Back-propagating fronts have also been identified during slow slip events (SSEs) in Cascadia and Japan, appearing as tremor swarms known as Rapid Tremor Reversals (RTR) which migrate at fast speed in the direction opposite to the propagation of the large-scale slow slip (Houston et al., 2011).

Here, we show that pulses can be generated by a highly damaged LVFZ, even without the dynamic effects of reflected waves. We follow two complementary approaches: static rupture scaling arguments (section 2) and quasi-dynamic earthquake cycle simulations (section 3). Our simulations also reveal that the quasi-static effects of a highly damaged LVFZ are sufficient to generate back-propagating fronts.

2. Scaling Arguments for Quasi-Static Pulse Generation

We consider a simple, tabular LVFZ model defined by a finite fault of length L bisecting a homogeneous low-rigidity layer, the damage zone, embedded in an intact medium (Figure 1). The LVFZ is specified by its half-thickness h and its damage level Δ defined by

$$\mu_d = (1 - \Delta)\mu \tag{1}$$

where μ_d and μ are the shear moduli of the LVFZ and intact medium, respectively. We consider anti-plane deformation. The model converges to two different homogeneous end-member models, depending on the fault zone thickness. When h/L is very small, the model approaches a homogeneous intact medium with shear modulus μ. When h/L is very large, the model tends to a homogeneous damaged medium with shear modulus $(1 - \Delta)\mu$.

Key effects of a LVFZ on rupture propagation are highlighted by analyzing the limiting case of a highly damaged fault zone ($\Delta \to 1$), which is asymptotically equivalent to the case of a rigid medium surrounding an elastic fault zone considered by Horowitz and Ruina (1989). We consider a rupture growing quasi-statically with prescribed uniform stress drop $\Delta\tau$ and increasing rupture half-length $r(t)$. The fault zone thickness h is fixed, and for illustrative purposes, we set $\Delta = 0.99$. The resulting slip profiles (Figure 1c) are computed by solving numerically a static problem in which we account for static stress interactions modified by the presence of the damaged layer, as described in supporting information Text S2. The shape of the slip profile is indicative of the style of rupture: Crack-like ruptures show an elliptical slip profile whereas (steady-state) pulses have a flat slip profile (Gabriel et al., 2012). While the rupture is small ($r(t) \ll h$), it only interacts with the damaged zone and therefore has a crack-like slip profile, as in a uniformly damaged infinite medium. Its slip grows proportional to rupture length as $\mathcal{D}(t) \sim \frac{\Delta\tau}{2\mu(1-\Delta)} r(t)$. As the rupture grows large ($r(t) \gg h$), it interacts with a thin elastic slab of thickness h and develops a pulse-like slip profile. Its slip reaches a value independent of rupture length, $\mathcal{D} \sim \frac{\Delta\tau}{\mu(1-\Delta)} h$, as expected in a thin slab problem. Connecting these two rupture stages together, a growing rupture with constant stress drop in a highly damaged LVFZ will initiate as a crack-like rupture and later transition into a pulse. The transition is characterized by saturation of slip caused by the LVFZ once the rupture grows larger than $2h$.

The above picture of crack-to-pulse transition provides insight into what controls rise time in a damaged fault zone in the absence of wave reflection effects. The rise time at the hypocenter is the time required for the appearance of a healing front. This time corresponds kinematically to the emergence of pulses, which is approximately the time required for the size of the initial crack to grow up to $r(t) = h$. Assuming a constant rupture speed v_r, the size of the rupture is $r(t) \sim v_r t$; hence, the rise time at the hypocenter roughly follows:

$$t \sim \frac{h}{v_r} \tag{2}$$

This estimation of rise time is valid at other locations beyond the hypocenter assuming that the propagation speed of the healing front is close to the rupture speed. Because rise time can be shorter away from the hypocenter (Huang & Ampuero, 2011), equation (2) should be taken as an upper bound. The resulting upper bound for the pulse width, defined as the distance between the position of the rupture front and the healing front, is as follows:

$$l \sim v_r t \sim h \tag{3}$$

The foregoing simplified analysis predicts the emergence of pulses from static effects alone, independently of the presence of reflected waves in the LVFZ.

3. Pulses and Back-Propagating Fronts in Quasi-Dynamic Multicycle Models

We conduct quasi-dynamic earthquake cycle simulations under rate-and-state friction (Text S1 for methods), covering a wide range of values of LVFZ thickness and damage. Our simulations do not include dynamical effects from reflected waves. Each simulation produces a history of seismic activity, including earthquakes with multiple sizes (Figure S1). The largest earthquakes in one simulation span the whole seismogenic length L_{vw} (Figure S2) and are labeled as characteristic events. In a given fault model, characteristic events have the same magnitude but may show different rupture patterns. We define an earthquake cycle as the period between two characteristic events. In some fault models, simulations show a variable duration of the earthquake cycle. We only consider results in characteristic events after a spin-up period of several initial cycles, avoiding a dependence of our results on the arbitrarily prescribed initial conditions.

Complex slip patterns appear in characteristic events when damage is high ($\Delta > 0.7$), and the fault zone is thin compared to the length of the seismogenic zone ($2h < L_{vw}$). Two signatures characterize the slip complexity: the promotion of pulses (Figure 2a) and the rerupture of previously healed fault segments during the same event (Figures 2b and 2e).

Pulses are defined here by a drastic reduction of slip rate ($V < 1$ cm/s) at a short distance behind the rupture front, leading to a short rise time. We observe a systematic reduction of the average rise time over a wide range of LVFZ thickness and high damage values (Figure 2a). Short rise times occur roughly within the range of LVFZ parameters that produce flat slip profiles in the static rupture models computed in section 2 (Figure 2a), consistent with the kinematic implications we drew from the static crack analysis.

The rerupture of previously healed fault segments (Figure 2b) is characterized by the emergence of secondary fronts propagating in the opposite direction to the main rupture front (Figures 2e and S3). These back-propagating fronts have a short rise time and can rerupture multiple times the same fault segment. Models with seismogenic zones that are much larger than the nucleation size ($L_{vw} \gg L_{nuc}$; Text S1) promote back-propagating fronts without requiring a LVFZ, but their rise time is longer, and their number of reruptures is small (Figure 2f with $L_{vw} \sim 100 L_{nuc}$).

In addition to characteristic events with complex slip patterns, events comprising a wide range of sizes develop in thick and highly damaged fault zones (Figure 2c), where small events partially break the seismogenic zone from the edges (Figure S1). Small, noncharacteristic events are known to emerge in rate-and-state friction models in homogeneous media with seismogenic zones much larger than their nucleation length L_{nuc} (Barbot, 2019; Cattania, 2019). The nucleation length is the smallest size of a slip patch that can accelerate to instability (Rubin & Ampuero, 2005). In a homogeneous medium, it is proportional to the shear modulus, and in a damaged zone to a reduced, effective shear modulus that depends on h and Δ (Text S1). The LVFZ thickness and damage values promoting variable event magnitudes in our models are well explained by the increase in the L_{vw}/L_{nuc} ratio due to the reduction in L_{nuc} induced by the LVFZ (Figure 2c). The smallest nucleation length is achieved in models with $\Delta = 0.9$ and $2h > L_{vw}$, which have $L_{vw} \sim 100 L_{nuc}$.

The rupture speed in our homogeneous medium model (Figure 2d) corresponds to $V_{rup} \sim 1$ km/s, a typical value in seismological observations. In contrast, a highly damaged fault zone promotes a reduction in the rupture speed $V^d_{rup}/V_{rup} \propto (1 - \Delta)$, compatible with theoretical quasi-static predictions of rupture speed (Ampuero & Rubin, 2008) but slower than most seismological observations. The nondimensional units in Figure 2 can be converted into real scales depending on the assumed value of the characteristic slip distance of rate-and-state friction, D_c; examples of dimensional scales are given in Table S1 for $D_c = 2$ mm.

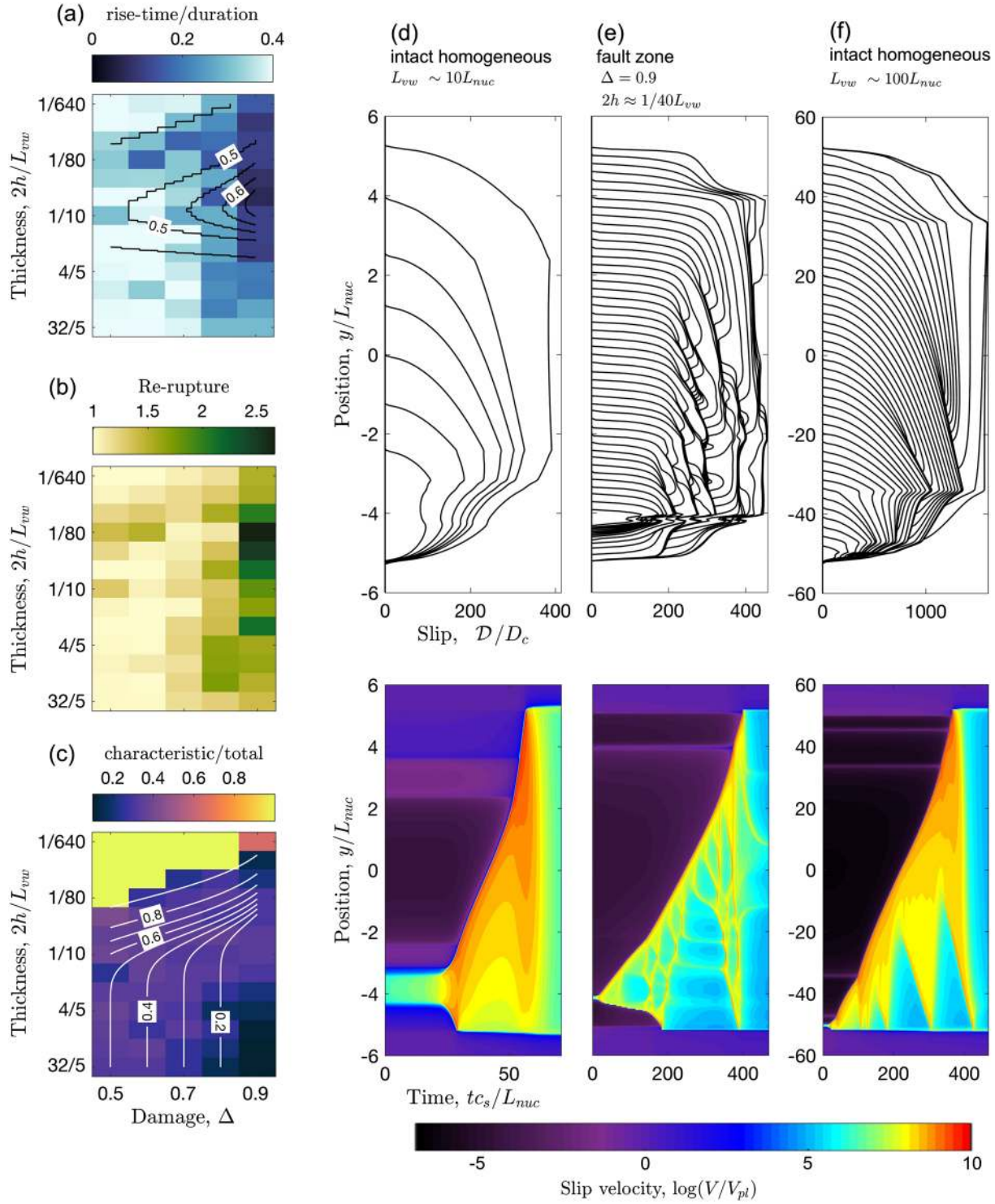

Figure 2. Properties of ruptures and seismicity in fault zone models after multiple earthquake cycles and spatiotemporal evolution of slip and slip velocity in the characteristic event of earthquake cycle models. (a) Average rise time normalized by the total rupture duration, (b) average number of rupture fronts ($V > 1$ cm/s) during an event, and (c) number of characteristic events over the total number of events as a function of damage level Δ and fault zone thickness $2h$ normalized by the size of the velocity-weakening fault segment L_{vw}. The rise time is defined here as the duration of slip rate exceeding 1 cm/s. Black contour lines in (a) are a semianalytical prediction of the flatness of the slip profile in a constant stress drop model (Text S2). The slip profiles are obtained with the same method used in Figure 1c. Flatness is the fraction of the fault length where slip is roughly constant, at most 20% lower than the maximum slip in the slip profile. The white contours in (c) show the estimated reduction of the nucleation length due to the LVFZ (contours of L_{nuc} in LVFZ normalized by its value in a homogeneous intact medium). (d) Spatiotemporal evolution of slip and slip velocity in the characteristic event of an intact homogeneous medium, (e) an LVFZ with $\Delta = 0.9$ and $2h \approx L_{vw}/40$, and (f) an intact homogeneous medium with ten times smaller nucleation length than (d).

4. Discussion

4.1. Short-Range Stress Transfer and the Origin of Pulses in an LVFZ

Models with nearest-neighbor stress transfer, such as the Burridge-Knopoff (BK) model (Burridge & Knopoff, 1967), have been often used as a mechanical analog to earthquake rupture and are capable of promoting pulses in the continuum limit (Brener et al., 2018; Erickson et al., 2011). In a BK model, a chain of sliders connected by springs is loaded by a uniform displacement applied to a loading spring (Burridge & Knopoff, 1967). In a uniform stress drop rupture, the BK model produces the flat static slip profile characteristic of pulses when the loading stiffness is much higher than the static stress transfer due to the relative motion of sliders (Text S3). Under our current model parameters (Table S2), ruptures propagate as pulses both in a nearest-neighbor model (Figure 3a) and in a fault zone model with large damage, $\Delta = 0.9$ (Figure 2e). Here we show that the emergence of pulses in an LVFZ can be related to stress interactions approaching the nearest-neighbor regime across a wide range of slip wavelengths.

The static stress transfer in a fault zone model due to spatially harmonic slip with wavelength k and unit amplitude is (Text S2 and Figure S4):

$$\mathcal{K}(k) = \frac{1}{2}\mu(1-\Delta)|k| \coth\left(h|k| + \operatorname{atanh}(1-\Delta)\right) \tag{4}$$

Asymptotic analysis (Figure 4a and Text S3) shows that at low k the stress transfer in an LVFZ tends to that of an intact homogeneous medium, whereas at high k it tends to that of a damaged homogeneous medium. In an intermediate range of wavelengths, the stress transfer is approximately nearest-neighbor. As Δ increases, the relative bandwidth of the nearest-neighbor regime broadens (Figure S8), and the short rise time observed in the nearest-neighbor model (Figure 3a) appears in the LVFZ model as well. In other words, increasing the LVFZ damage level extends the range of slip length scales where pulses can exist. When h is small ($h \ll \sqrt{3}L_{vw}$), an LVFZ model within the nearest-neighbor regime produces uniform stress drop ruptures with a slip profile that is flat and has an average slip $D \approx 2h\Delta\tau/\mu(1-\Delta)$ (Text S3).

The limiting case where $\Delta \to 1$, analyzed in section 2, represents an elastic layer of thickness $2h$ bounded by an infinitely rigid medium (Horowitz & Ruina, 1989). Stress interactions in that case are nearest-neighbor at wavelengths larger than $\sim 2\pi h$ (Figure S8). Such model is completely nearest-neighbor if the process zone size, the smallest characteristic length scale of slip, is larger than $\sim 2\pi h$.

4.2. Origin of Back-Propagating Fronts

Highlighted in our work as a manifestation of rupture complexity, back-propagating fronts owe part of their relevance to recent earthquake observations. A recent report from an M7.1 oceanic transform earthquake features a "boomerang earthquake" slip pattern (Hicks et al., 2020) that resembles the structure of back-propagating fronts shown in our models. Seismic observations indicate that LVFZs extend throughout the seismogenic zone in oceanic transform faults (Roland et al., 2012), enhancing the relevance of our model to explain the "boomerang earthquake" slip pattern. In a different tectonic setting, a back-propagating front appears during a recently reported M8 intermediate-depth earthquake (Vallée et al., 2020). Both observations are independently supported by teleseismic back-projection imaging and finite source inversion, suggesting the ubiquity of back-propagating fronts to different tectonic environments.

The static solutions introduced in section 2 provide insight on the origin of multiple back-propagating fronts. Relying on an idealized situation where the only deformable medium is within the LVFZ, we showed the emergence of a transition from a crack into a pulse when the rupture size exceeds $2h$. In reality the medium outside the LVFZ is deformable as well. As the rupture continues growing to sizes much larger than $2h$, stress increasingly transfers through the outer medium. Eventually, the influence of the LVFZ becomes irrelevant to the propagation of the rupture. At this point, the static analysis predicts a second, reverse transition from pulse-like behavior to the crack-like behavior of an intact homogeneous medium (Figure 4b). Beyond this transition, slip increases in regions that were previously healed. Therefore, slip reactivation is required there, leading to secondary rupture fronts.

We expect reruptures to initiate where stresses are the highest, which is near the primary rupture front; thus, the ensuing secondary rupture fronts have to propagate backwards. Furthermore, because these secondary ruptures start small, they need to go through a pulse-like phase. In summary, in the presence of an LVFZ, back-propagating pulses are necessary to complete the slip budget of a very large rupture, filling the slip gap between intermediate-size pulses and large-size cracks.

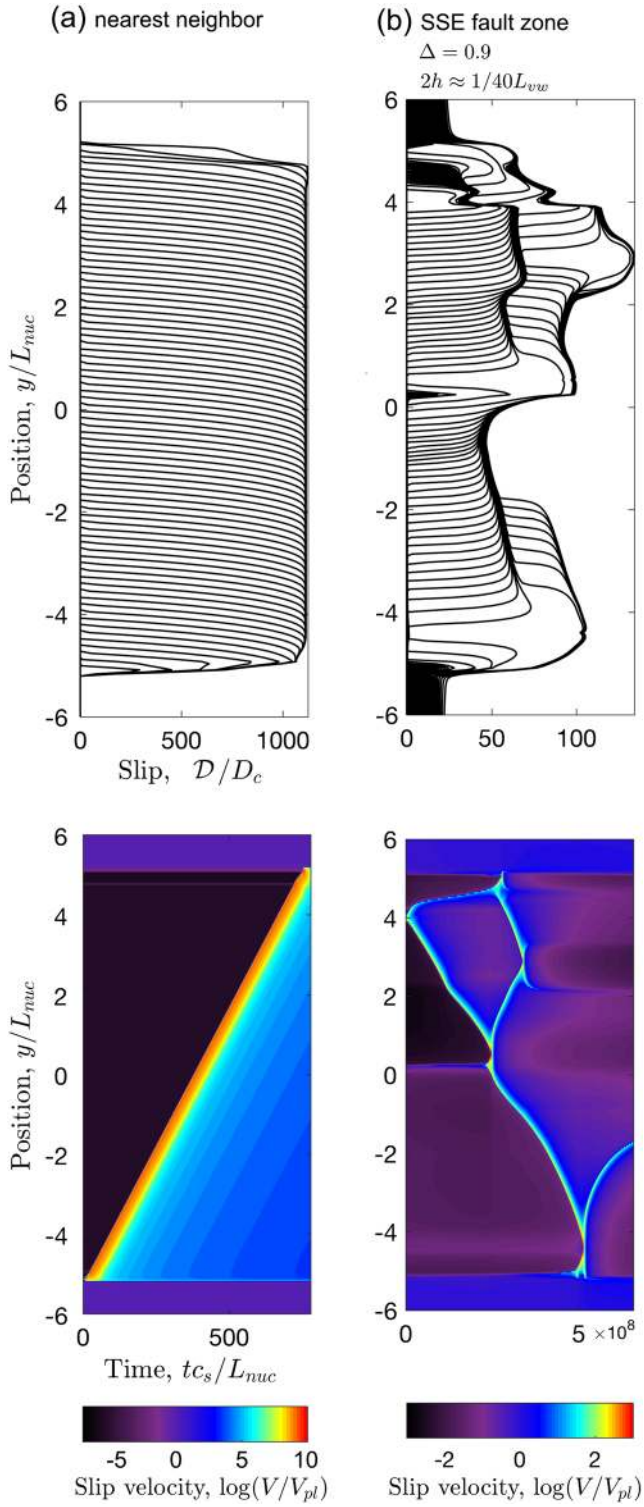

Figure 3. Spatiotemporal evolution of slip and slip rate in the characteristic event of earthquake cycle models assuming (a) a nearest-neighbor model with $\Delta = 0.99$ and $2h = L_{vw}/25$ and (b) a slow-slip model in a LVFZ model with $\Delta = 0.9$ and $2h \approx L_{vw}/40$ and a modified friction law with velocity strengthening at high velocities. Axes are normalized following the convention in Figure 2.

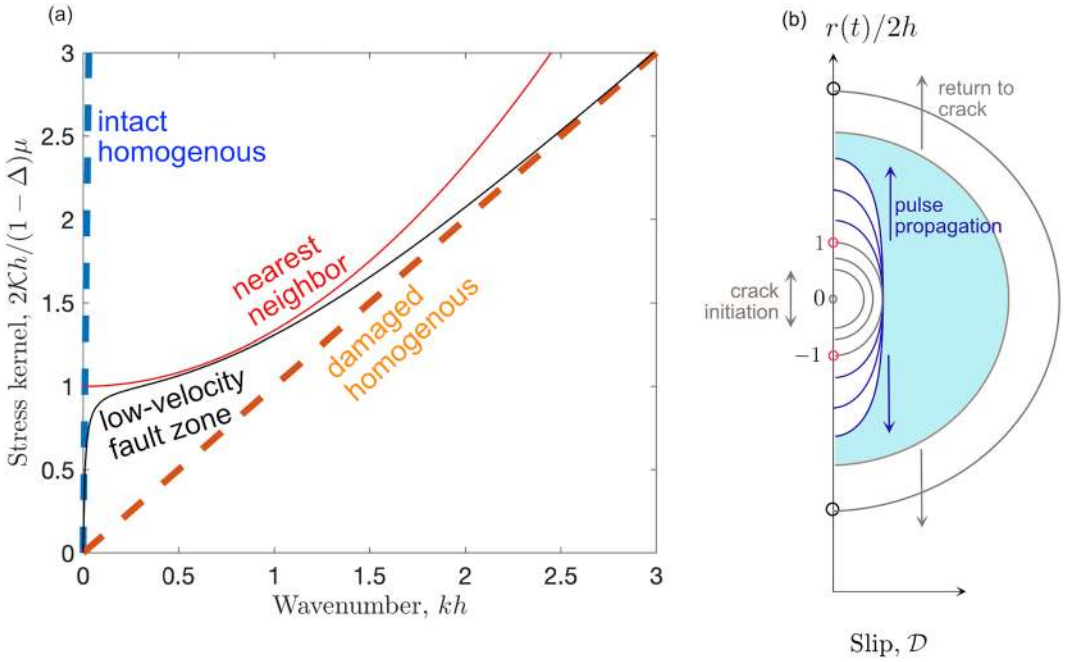

Figure 4. Nearest-neighbor stress transfer and promotion of slip complexity. (a) The static stress transfer kernel of an LVFZ (Equation 4) with $\Delta = 0.99$ (black) in Fourier domain, as a function of the normalized wavenumber kh of slip, and its nearest-neighbor approximation (red) (Text S3). Also shown are the asymptotic limits of a homogeneous intact medium (blue dashed) ($\mathcal{K} = \mu|k|/2$) and homogeneous damaged medium (orange dashed) ($\mathcal{K} = \mu_d|k|/2$). The exaggerated level of damage $\Delta = 0.99$ represents the asymptotic limit of an LVFZ as damage increases. (b) Conceptual interpretation of the emergence of secondary pulses. Rerupturing is necessary to fill the slip deficit (cyan) between a pulse at intermediate rupture length ($r(t) > 2h$, purple curves) and a crack appearing at much larger lengths ($r(t) \gg 2h$, gray curves).

4.3. A Mechanism for RTRs

While observations of back-propagating fronts during earthquakes are challenging and still incipient, slow slip and tremor phenomena offer a unique and systematic opportunity to observe complex slip patterns in slow motion. The back-propagating fronts identified in Figure 2e suggest that a highly compliant LVFZ can provide a mechanism for RTRs observed in Cascadia and Japan during SSEs (Houston et al., 2011). Seismological observations suggest that subduction megathrusts are surrounded by low-velocity zones (Audet & Schaeffer, 2018; Nedimović et al., 2003) that are several kilometers thick near the region where tremor activity concentrates (Calvert et al., 2020). Instead of damaged rock, low-velocity zones in subduction zones mostly relate to layers of subducted material containing pressurized fluids. Previous models of RTR rely on frictional heterogeneities (Luo & Ampuero, 2017; Luo & Liu, 2019), pore fluid pressure waves (Cruz-Atienza et al., 2018), or external transient forcings such as tides (Hawthorne & Rubin, 2013b). Our models show RTR-like patterns emerging from a different mechanism: the quasi-static stress transfer of an LVFZ. Due to the ubiquity of LVFZ to both regular earthquakes and SSEs, our model supports the idea that detailed observations of slow slip phenomena contribute to understand earthquakes in general (Michel et al., 2019).

Our simulations show that back-propagating fronts also occur in slow slip models with an LVFZ (Figure 3b). Introducing strengthening at high slip rate is a known approach to model SSEs (Hawthorne & Rubin, 2013a). We added a linear velocity-strengthening term into the friction law (i.e., the fault strengthens proportionally to V), which is stronger than the logarithmic strengthening term of the conventional rate-and-state friction (Text S1). We chose a velocity-strengthening coefficient 10^6 times larger than the radiation damping coefficient. Our results indicate that back-propagating fronts emerge during SSEs in a LVFZ model with the modified friction, although they are less vigorous than those observed in our fast-rupture results (Figure 3). SSEs only show pulse-like behavior and back-propagating fronts in the presence of an LVFZ (Figure S5). As slow-slip models are insensitive to dynamical effects, our results confirm that back-propagating fronts emerge from quasi-static LVFZ effects alone. The SSE propagation speed in our model is ~5 m/day, about 1,000 times lower than SSE propagation speeds observed in Cascadia, which range from 7 to 15 km/day

(Houston et al., 2011). Further work is required to examine how low-velocity zones quantitatively affect tremor migration patterns in more detailed slow-slip models.

The damage level observed in strike-slip faults ranges from 0.45 to 0.85 and the fault zone thickness from 80 to 1,500 m, with typical values $\Delta \sim 0.65$ and $2h \sim 200$ m (Figure S6). The most damaged fault zone structures reach $\Delta \sim 0.85$ (Li et al., 2007; Yang & Zhu, 2010), which is close to the minimum value required by our model to show significant slip complexity (Figures 2a and 2b). For $\Delta \sim 0.85$ and a reasonable fault zone thickness $2h$ from 100 m to 1 km, the rupture length required to develop pulses and back-propagating fronts must be larger than 2 to 20 km (Figures 2a and 2b). It is likely then that the quasi-static LVFZ effects described here do not operate during very small SSEs. The properties of fault zones where RTRs are observed are harder to be resolved compared to crustal faults due to the larger depths involved. Dimensions of fault zones in subduction environments have been inferred from observations in exhumed subduction zones (Rowe et al., 2013), but their elastic properties remain poorly constrained. Receiver functions suggest that the v_p/v_s ratio may increase over ~75% due to overpressurization of fluids within the several-km-thick low-velocity zone that surrounds regions where tremors are generated (Audet & Schaeffer, 2018; Calvert et al., 2020).

4.4. Potential Model Limitations

Further research is warranted to investigate whether the effects observed in our idealized fault zone model remain after releasing some of the simplifying assumptions, in particular the quasi-dynamic approximation and the 2-D tabular LVFZ geometry.

Quasi-dynamic simulations in the absence of a LVFZ qualitatively agree with fully dynamic simulations under a conventional Dieterich-Ruina friction law (Thomas et al., 2014). However, dynamic simulations that include an LVFZ produce a range of fault zone waves, including reflected, trapped, and head waves (Huang & Ampuero, 2011; Huang et al., 2014), which can perturb the dynamic stress on the fault and interfere with the quasi-static mechanism highlighted in the present work. Preliminary results suggest that dynamic effects modulate but do not obliterate the quasi-static effects reported here (Flores-Cuba et al., 2020). Similarly, in previous dynamic single-rupture simulations (Huang et al., 2014) dynamic LVFZ wave effects modulate, but do not obliterate the generation of pulses by another mechanism, enhanced velocity-weakening friction. An important open question is whether the dynamic effects of fault zone waves allow the slip complexity revealed here to operate over a broader range of LVFZ property values, including the lower, commonly observed levels of fault zone damage.

The direction of slip is not important in the context of our quasi-dynamic model. Our anti-plane results can be transferred to in-plane slip by replacing μ with $\mu/(1-\nu)$, where ν is Poisson's ratio. However, in-plane dynamical models can promote additional slip complexity, for instance transitions to supershear rupture speed which are relevant for the interpretation of past earthquakes (Huang et al., 2016; Oral et al., 2020).

The 3-D structure of damage zones observed in the field is more complicated than a simple 2-D tabular region, usually displaying flower structures with wider thickness at shallower depth (Finzi et al., 2009; Mitchell & Faulkner, 2009; Savage & Brodsky, 2011). Moreover, LVFZ properties are not uniform along strike as the fault zone thickness varies with along-strike changes in fault geometry and the total amount of slip locally accumulated over time (Ampuero & Mao, 2017; Mitchell & Faulkner, 2009; Perrin et al., 2016). How such systematic variations of LVFZ properties affect the rupture features highlighted here warrants further study. We expect that the promotion by LVFZ of pulses and back-propagating fronts reported in our 2-D simulations should also appear in 3-D simulations, as the static transfer mechanism is approximately the same (similar to Equation 4 with k replaced by the modulus of the wavenumber vector).

The quasi-static pulse-generation mechanism revealed here should persist in a LVFZ without the sharp elasticity contrasts of a simple tabular damage zone, in contrast to the dynamic mechanism of pulse-generation by reflected waves (Huang et al., 2014). In fact, the static stress transfer in a model with exponential decay of damage as a function of distance from the fault (Ampuero et al., 2002) has the same essential features as in our tabular model (Equation 4), in particular the same asymptotic behaviors highlighted in Figure 4.

5. Conclusions

Our analytical arguments and simulation results show that rupture pulses emerge and persist across multiple earthquake cycles via quasi-static effects in a fault surrounded by a highly damaged fault zone,

independently of the dynamic effects induced by fault zone-reflected waves. We develop a formal analogy between a fault zone model and a nearest-neighbor (BK) model that explains the emergence of pulses. Nearest-neighbor models are known to produce pulses, and within a certain range of length scales, the stress transfer in a damaged fault zone is approximately nearest-neighbor. Our results suggest that the earthquake rise time should be proportional to fault zone thickness divided by rupture speed in highly damaged faults.

We also showed that fault zone effects can produce complex slip patterns, including back-propagating fronts that rerupture previously healed fault segments. Such back-propagating fronts have been most recently observed in large earthquakes. The back-propagating fronts in our slow-slip models with highly damaged fault zones are also analogous to RTRs observed in Cascadia and Japan.

Overall, quasi-static fault zone effects provide a simple mechanism to promote and sustain earthquake complexity and a mechanical link between structural fault properties and seismicity. Our results further motivate the quest for higher temporal and spatial resolution in earthquake source studies. The systematic exploration of model parameters contained in our results provide targets for laboratory experiments aimed at understanding the interactions between rupture propagation and heterogeneous media.

Data Availability Statement

Data sharing is not applicable to this article as no data sets were generated or analyzed during the current study. The Quasi-DYNamic earthquake simulator (QDYN) (Luo et al., 2017) used to compute our numerical models of earthquake cycles is available online (github.com/ydluo/qdyn). QDYN is freely available for academic research purposes and licensed by GNU General Public License, Version 3.

Acknowledgments
This work was supported by the Southern California Earthquake Center (SCEC) and by the French government through the FAULTS_R_GEMS project (ANR-17-CE31-0008) and the UCAJEDI Investments in the Future project (ANR-15-IDEX-01) managed by the National Research Agency (ANR). SCEC is funded by NSF Cooperative Agreement EAR-1600087 and USGS Cooperative Agreement G17AC00047. This is SCEC Contribution No. 10084.

References

Aagaard, B. T., & Heaton, T. H. (2008). Constraining fault constitutive behavior with slip and stress heterogeneity. *Journal of Geophysical Research*, *113*, B04301. https://doi.org/10.1029/2006JB004793

Ampuero, J. P., & Mao, X. (2017). Upper limit on damage zone thickness controlled by seismogenic depth. *Fault Zone Dynamic Processes: Evolution of Fault Properties During Seismic Rupture*, *227*, 243.

Ampuero, J.-P., & Rubin, A. M. (2008). Earthquake nucleation on rate and state faults–aging and slip laws. *Journal of Geophysical Research*, *113*, B01302. https://doi.org/10.1029/2007JB005082

Ampuero, J.-P., Vilotte, J.-P., & Sanchez-Sesma, F. J. (2002). Nucleation of rupture under slip dependent friction law: Simple models of fault zone. *Journal of Geophysical Research*, *107*(B12), 2324. https://doi.org/10.1029/2001JB000452

Audet, P., & Schaeffer, A. J. (2018). Fluid pressure and shear zone development over the locked to slow slip region in Cascadia. *Science Advances*, *4*(3), eaar2982.

Barbot, S. (2019). Slow-slip, slow earthquakes, period-two cycles, full and partial ruptures, and deterministic chaos in a single asperity fault. *Tectonophysics*, *768*, 228171.

Ben-Zion, Y., Peng, Z., Okaya, D., Seeber, L., Armbruster, J. G., Ozer, N., et al. (2003). A shallow fault-zone structure illuminated by trapped waves in the Karadere–Duzce branch of the North Anatolian Fault, western Turkey. *Geophysical Journal International*, *152*(3), 699–717.

Beroza, G. C., & Mikumo, T. (1996). Short slip duration in dynamic rupture in the presence of heterogeneous fault properties. *Journal of Geophysical Research*, *101*(B10), 22,449–22,460.

Beroza, G. C., & Spudich, P. (1988). Linearized inversion for fault rupture behavior: Application to the 1984 Morgan Hill, California, earthquake. *Journal of Geophysical Research*, *93*(B6), 6275–6296.

Brener, E. A., Aldam, M., Barras, F., Molinari, J.-F., & Bouchbinder, E. (2018). Unstable slip pulses and earthquake nucleation as a nonequilibrium first-order phase transition. *Physical Review Letters*, *121*(23), 234302.

Burridge, R., & Knopoff, L. (1967). Model and theoretical seismicity. *Bulletin of the Seismological Society of America*, *57*(3), 341–371.

Calvert, A. J., Bostock, M. G., Savard, G., & Unsworth, M. J. (2020). Cascadia low frequency earthquakes at the base of an overpressured subduction shear zone. *Nature Communications*, *11*(1), 1–10.

Cattania, C. (2019). Complex earthquake sequences on simple faults. *Geophysical Research Letters*, *46*, 10,384–10,393. https://doi.org/10.1029/2019GL083628

Chester, F. M., & Logan, J. M. (1986). Implications for mechanical properties of brittle faults from observations of the Punchbowl fault zone, California. *Pure and Applied Geophysics*, *124*(1–2), 79–106.

Cochard, A., & Madariaga, R. (1996). Complexity of seismicity due to highly rate-dependent friction. *Journal of Geophysical Research*, *101*(B11), 25,321–25,336.

Cochran, E. S., Li, Y.-G., Shearer, P. M., Barbot, S., Fialko, Y., & Vidale, J. E. (2009). Seismic and geodetic evidence for extensive, long-lived fault damage zones. *Geology*, *37*(4), 315–318.

Cruz-Atienza, V. M., Villafuerte, C., & Bhat, H. S. (2018). Rapid tremor migration and pore-pressure waves in subduction zones. *Nature Communications*, *9*(1), 1–13.

Day, S. M. (1982). Three-dimensional finite difference simulation of fault dynamics: Rectangular faults with fixed rupture velocity. *Bulletin of the Seismological Society of America*, *72*(3), 705–727.

Day, S. M., Yu, G., & Wald, D. J. (1998). Dynamic stress changes during earthquake rupture. *Bulletin of the Seismological Society of America*, *88*(2), 512–522.

Erickson, B. A., Birnir, B., & Lavallée, D. (2011). Periodicity, chaos and localization in a Burridge–Knopoff model of an earthquake with rate-and-state friction. *Geophysical Journal International*, *187*(1), 178–198.

Finzi, Y., Hearn, E. H., Ben-Zion, Y., & Lyakhovsky, V. (2009). Structural properties and deformation patterns of evolving strike-slip faults: Numerical simulations incorporating damage rheology. *Pure and Applied Geophysics*, *166*(10–11), 1537–1573.

Flores-Cuba, J. M., Ampuero, J.-P., Oral, E., & Idini, B. (2020). Fault damage zones enhance earthquake rupture complexity over multiple cycles. Abstract S036-0004 presented at 2020 AGU Fall Meeting, 1–17 Dec.

Gabriel, A.-A., Ampuero, J.-P., Dalguer, L. A., & Mai, P. M. (2012). The transition of dynamic rupture styles in elastic media under velocity-weakening friction. *Journal of Geophysical Research*, *117*, B09311. https://doi.org/10.1029/2012JB009468

Harris, R. A., & Day, S. M. (1997). Effects of a low-velocity zone on a dynamic rupture. *Bulletin of the Seismological Society of America*, *87*(5), 1267–1280.

Hawthorne, J. C., & Rubin, A. M. (2013a). Laterally propagating slow slip events in a rate and state friction model with a velocity-weakening to velocity-strengthening transition. *Journal of Geophysical Research: Solid Earth*, *118*, 3785–3808. https://doi.org/10.1002/jgrb.50261

Hawthorne, J. C., & Rubin, A. M. (2013b). Tidal modulation and back-propagating fronts in slow slip events simulated with a velocity-weakening to velocity-strengthening friction law. *Journal of Geophysical Research: Solid Earth*, *118*, 1216–1239. https://doi.org/10.1002/jgrb.50107

Heaton, T. H. (1990). Evidence for and implications of self-healing pulses of slip in earthquake rupture. *Physics of the Earth and Planetary Interiors*, *64*(1), 1–20.

Hicks, S. P., Okuwaki, R., Steinberg, A., Rychert, C. A., Harmon, N., Abercrombie, R. E., et al. (2020). Back-propagating supershear rupture in the 2016 M w 7.1 Romanche transform fault earthquake. *Nature Geoscience*, *13*, 647–653.

Horowitz, F. G., & Ruina, A. (1989). Slip patterns in a spatially homogeneous fault model. *Journal of Geophysical Research*, *94*(B8), 10,279–10,298.

Houston, H., Delbridge, B. G., Wech, A. G., & Creager, K. C. (2011). Rapid tremor reversals in Cascadia generated by a weakened plate interface. *Nature Geoscience*, *4*(6), 404.

Huang, Y., & Ampuero, J.-P. (2011). Pulse-like ruptures induced by low-velocity fault zones. *Journal of Geophysical Research*, *116*, B12307. https://doi.org/10.1029/2011JB008684

Huang, Y., Ampuero, J.-P., & Helmberger, D. V. (2014). Earthquake ruptures modulated by waves in damaged fault zones. *Journal of Geophysical Research: Solid Earth*, *119*, 3133–3154. https://doi.org/10.1002/2013JB010724

Huang, Y., Ampuero, J.-P., & Helmberger, D. V. (2016). The potential for supershear earthquakes in damaged fault zones–theory and observations. *Earth and Planetary Science Letters*, *433*, 109–115.

Idini, B., & Ampuero, J.-P. (2017). Rupture complexity promoted by damaged fault zones in earthquake cycle models. *Earth and Space Science Open Archive*, *110*(2011), 10500080. https://doi.org/10.1002/essoar.10500080.1

Johnson, E. (1990). On the initiation of unidirectional slip. *Geophysical Journal International*, *101*(1), 125–132.

Lewis, M. A., & Ben-Zion, Y. (2010). Diversity of fault zone damage and trapping structures in the Parkfield section of the San Andreas Fault from comprehensive analysis of near fault seismograms. *Geophysical Journal International*, *183*(3), 1579–1595.

Lewis, M. A., Peng, Z., Ben-Zion, Y., & Vernon, F. L. (2005). Shallow seismic trapping structure in the San Jacinto fault zone near Anza, California. *Geophysical Journal International*, *162*(3), 867–881.

Li, Y.-G., Chen, P., Cochran, E. S., Vidale, J. E., & Burdette, T. (2006). Seismic evidence for rock damage and healing on the San Andreas fault associated with the 2004 m 6.0 parkfield earthquake. *Bulletin of the Seismological Society of America*, *96*(4B), S349–S363.

Li, Y.-G., Leary, P., Aki, K., & Malin, P. (1990). Seismic trapped modes in the oroville and san andreas fault zones. *Science*, *249*(4970), 763–766.

Li, Y.-G., Vidale, J. E., Day, S. M., & Oglesby, D. D. (2002). Study of the 1999 M 7.1 Hector Mine, California, earthquake fault plane by trapped waves. *Bulletin of the Seismological Society of America*, *92*(4), 1318–1332.

Li, H., Zhu, L., & Yang, H. (2007). High-resolution structures of the Landers fault zone inferred from aftershock waveform data. *Geophysical Journal International*, *171*(3), 1295–1307.

Luo, Y., & Ampuero, J.-P. (2017). Tremor migration patterns and the collective behavior of deep asperities mediated by creep.

Luo, Y., Ampuero, J.-P., Galvez, P., van den Ende, M., & Idini, B. (2017). QDYN: A Quasi-DYNamic earthquake simulator (v1.1). Zenodo. https://doi.org/10.5281/zenodo.322459

Luo, Y., & Liu, Z. (2019). Rate-and-state model casts new insight into episodic tremor and slow-slip variability in cascadia. *Geophysical Research Letters*, *46*, 6352–6362. https://doi.org/10.1029/2019GL082694

Meng, L., Ampuero, J. P., Page, M. T., & Hudnut, K. W. (2011). Seismological evidence and dynamic model of reverse rupture propagation during the 2010 M7. 2 El Mayor Cucapah earthquake. Abstract S52B-04 presented at 2011 Fall Meeting, AGU, San Francisco, CA, 5–9 Dec.

Meng, L., Ampuero, J.-P., Stock, J., Duputel, Z., Luo, Y., & Tsai, V. C. (2012). Earthquake in a maze: Compressional rupture branching during the 2012 Mw 8.6 Sumatra earthquake. *Science*, *337*(6095), 724–726.

Michel, S., Gualandi, A., & Avouac, J.-P. (2019). Similar scaling laws for earthquakes and Cascadia slow-slip events. *Nature*, *574*(7779), 522–526.

Mitchell, T. M., & Faulkner, D. R. (2009). The nature and origin of off-fault damage surrounding strike-slip fault zones with a wide range of displacements: A field study from the Atacama fault system, northern Chile. *Journal of Structural Geology*, *31*(8), 802–816.

Mizuno, T., Kuwahara, Y., Ito, H., & Nishigami, K. (2008). Spatial variations in fault-zone structure along the Nojima fault, central Japan, as inferred from borehole observations of fault-zone trapped waves. *Bulletin of the Seismological Society of America*, *98*(2), 558–570.

Nedimović, M. R., Hyndman, R. D., Ramachandran, K., & Spence, G. D. (2003). Reflection signature of seismic and aseismic slip on the northern cascadia subduction interface. *Nature*, *424*(6947), 416.

Nielsen, S., & Madariaga, R. (2003). On the self-healing fracture mode. *Bulletin of the Seismological Society of America*, *93*(6), 2375–2388.

Noda, H., Dunham, E. M., & Rice, J. R. (2009). Earthquake ruptures with thermal weakening and the operation of major faults at low overall stress levels. *Journal of Geophysical Research*, *114*, B07302. https://doi.org/10.1029/2008JB006143

Oral, E., Weng, H., & Ampuero, J. P. (2020). Does a damaged-fault zone mitigate the near-field impact of supershear earthquakes?—Application to the 2018 7.5 Palu, Indonesia, earthquake. *Geophysical Research Letters*, *47*, e2019GL085649. https://doi.org/10.1029/2019GL085649

Peng, Z., Ben-Zion, Y., Michael, A. J., & Zhu, L. (2003). Quantitative analysis of seismic fault zone waves in the rupture zone of the 1992 Landers, California, earthquake: Evidence for a shallow trapping structure. *Geophysical Journal International*, *155*(3), 1021–1041.

Perrin, C., Manighetti, I., Ampuero, J.-P., Cappa, F., & Gaudemer, Y. (2016). Location of largest earthquake slip and fast rupture controlled by along-strike change in fault structural maturity due to fault growth. *Journal of Geophysical Research: Solid Earth*, *121*, 3666–3685. https://doi.org/10.1002/2015JB012671

Perrin, G., Rice, J. R., & Zheng, G. (1995). Self-healing slip pulse on a frictional surface. *Journal of the Mechanics and Physics of Solids*, *43*(9), 1461–1495.

Roland, E., Lizarralde, D., McGuire, J. J., & Collins, J. A. (2012). Seismic velocity constraints on the material properties that control earthquake behavior at the Quebrada-Discovery-Gofar transform faults, east pacific rise. *Journal of Geophysical Research*, *117*, B11102. https://doi.org/10.1029/2012JB009422

Ross, Z. E., Idini, B., Jia, Z., Stephenson, O. L., Zhong, M., Wang, X., et al. (2019). Hierarchical interlocked orthogonal faulting in the 2019 Ridgecrest earthquake sequence. *Science*, *366*(6463), 346–351.

Rowe, C. D., Moore, J. C., Remitti, F., & Scientists, IODPET (2013). The thickness of subduction plate boundary faults from the seafloor into the seismogenic zone. *Geology*, *41*(9), 991–994.

Rubin, A. M., & Ampuero, J.-P. (2005). Earthquake nucleation on (aging) rate and state faults. *Journal of Geophysical Research*, *110*, B11312. https://doi.org/10.1029/2005JB003686

Savage, H. M., & Brodsky, E. E. (2011). Collateral damage: Evolution with displacement of fracture distribution and secondary fault strands in fault damage zones. *Journal of Geophysical Research*, *116*, B03405. https://doi.org/10.1029/2010JB007665

Thakur, P., Huang, Y., & Kaneko, Y. (2020). Effects of low-velocity fault damage zones on long-term earthquake behaviors on mature strike-slip faults. *Journal of Geophysical Research: Solid Earth*, *125*, e2020JB019587. https://doi.org/10.1029/2020JB019587

Thomas, M. Y., Lapusta, N., Noda, H., & Avouac, J.-P. (2014). Quasi-dynamic versus fully dynamic simulations of earthquakes and aseismic slip with and without enhanced coseismic weakening. *Journal of Geophysical Research: Solid Earth*, *119*, 1986–2004. https://doi.org/10.1002/2013JB010615

Uchide, T., Yao, H., & Shearer, P. M. (2013). Spatio-temporal distribution of fault slip and high-frequency radiation of the 2010 el Mayor-Cucapah, Mexico earthquake. *Journal of Geophysical Research: Solid Earth*, *118*, 1546–1555. https://doi.org/10.1002/jgrb.50144

Vallée, M., Grandin, R., Nocquet, J. M., Villegas, J. C., Vaca, S., Xie, Y., et al. (2020). Rupture characteristics of the 2019 North Peru intraslab earthquake (Mw8.0). Abstract S043-08 presented at 2020 AGU Fall Meeting, 1–17 Dec.

Yang, H., & Zhu, L. (2010). Shallow low-velocity zone of the San Jacinto fault from local earthquake waveform modelling. *Geophysical Journal International*, *183*(1), 421–432.

Yang, H., Zhu, L., & Cochran, E. S. (2011). Seismic structures of the calico fault zone inferred from local earthquake travel time modelling. *Geophysical Journal International*, *186*(2), 760–770.

References From the Supporting Information

Cochard, A., & Rice, J. R. (1997). A spectral method for numerical elastodynamic fracture analysis without spatial replication of the rupture event. *Journal of the Mechanics and Physics of Solids*, *45*(8), 1393–1418.

Dieterich, J. H. (1981). Constitutive properties of faults with simulated gouge. *Mechanical Behavior of Crustal Rocks: The Handin Volume*, *24*, 103–120.

Kaneko, Y., Ampuero, J.-P., & Lapusta, N. (2011). Spectral-element simulations of long-term fault slip: Effect of low-rigidity layers on earthquake-cycle dynamics. *Journal of Geophysical Research*, *116*, B10313. https://doi.org/10.1029/2011JB008395

Rice, J. R. (1993). Spatio-temporal complexity of slip on a fault. *Journal of Geophysical Research*, *98*(B6), 9885–9907.

Ruina, A. (1980). Friction laws and instabilities: A quasi-static analysis of some dry friction behaviour (Ph. D. thesis). Division of Engineering, Brown University.

Ruina, A. (1983). Slip instability and state variable friction laws. *Journal of Geophysical Research*, *88*(B12), 10,359–10,370.